

Cancer associated eIF1A mutants impair Rps3 and Rps10 binding and enhance scanning of cell cycle genes

Urmila Sehrawat¹, Femke Koning¹, Shaked Ashkenazi¹, Gil Stelzer², Dena Leshkowitz², Rivka Dikstein^{1*}

Running title: eIF1A promotes translation of cell cycle genes

Key words: Translation initiation, eIF1A, eIF1AX, 5'UTR, AUG context, Rps3, Rps10, eIF1.

¹Dept. of Biomolecular Sciences, The Weizmann Institute of Science, Rehovot 76100, Israel.

²Dept. of Life Sciences Core Facilities, The Weizmann Institute of Science, Rehovot 76100, Israel.

*Corresponding author: Tel: 972-8-9342117; E-mail: rivka.dikstein@weizmann.ac.il

Abstract

Protein synthesis is linked to cell proliferation and its deregulation contributes to cancer. eIF1A plays a key role in scanning and AUG selection and differentially affects translation of distinct mRNAs. Its unstructured N-terminal-tail (NTT) is frequently mutated in several malignancies. Here we report that eIF1A is essential for cell proliferation and cell-cycle progression. Ribosome-profiling of eIF1A knockdown cells revealed a substantial enrichment of cell-cycle mRNAs among the downregulated genes, which are predominantly characterized by lengthy 5'UTR. Conversely, eIF1A depletion caused a broad stimulation of 5'UTRs initiation at near-cognate AUG, unveiling a prominent role of eIF1A in suppressing 5'UTR translation. In addition, the AUG-context dependent auto-regulation of eIF1 is disrupted by eIF1A depletion suggesting for their cooperation in AUG-context discrimination and scanning. Importantly, cancer-associated eIF1A-NTT mutants augment eIF1A positive effect on long 5'UTR while hardly affecting AUG selection. Mechanistically, these mutations diminish eIF1A interaction with Rps3 and Rps10 implicated in scanning-arrest. Our findings suggest that reduced binding of eIF1A NTT mutants to the ribosome retains its open state and facilitate scanning of long 5'UTR-containing cell cycle genes.

Introduction

The process of protein synthesis is one of the most energy consuming cellular processes and is therefore under tight regulation by nutrients availability and various signal transduction pathways related to stress and cell proliferation (1). Both, cell proliferation and mRNA translation are dependent upon the same mitogenic signaling and are therefore strongly linked. Within the eukaryotic translation machinery, the cap-binding eIF4E protein is the major target for these signaling events. The contribution of other initiation factors to the control of cellular growth is largely unknown.

Translation of mRNA requires a complex apparatus consisting of mRNA, ribosomes, tRNAs and protein factors. mRNA translation is a cyclic process which can be divided into initiation, elongation, termination and recycling. Within this framework the initiation stage is considered a major regulatory target. This stage involves different initiation factors (eIFs) and different mRNA features, all of which play important roles in translational control. The predominant form of eukaryotic translation initiation depends on the m7G cap structure, present at the 5' end of the mRNA. In addition, the translation process involves 43S Pre-Initiation Complex (PIC) consisting of 40S ribosome + associated factors, attachment of the PIC to the mRNA, ribosomal scanning, start codon selection and subunit joining (2, 3).

The scanning process which is critical to translation initiation, is promoted by eIF1 and eIF1A (3, 4). Biochemical, genetic, and structural analyses established that eIF1 and eIF1A bind the 40S subunit near the P and A sites, respectively, and promote an open 40S conformation which is scanning competent (3). The open conformation is supported by the C-terminal tail (CTT) of eIF1A. Base pairing of Met-tRNA_i with an AUG triplet promotes dissociation of eIF1 from the 40S subunit, rearrangement to a closed conformation and scanning arrest. The 'closed' arrested conformation of the 40S is facilitated by the N-terminal

tail (NTT) of eIF1A. Thus, the two tails of eIF1A play opposing roles in scanning and AUG selection. We have recently shown that the interaction of eIF1A with the 43S is partly mediated by Rps3 and Rps10, ribosomal proteins located at the A site, which undergo conformational change during transition of the 43S to 80S (5). How these interactions contribute to the initiation process is presently unknown.

eIF1A is a small 17 KD initiation factor that is highly conserved among all eukaryotes. Most of our knowledge on eIF1A function and structure was gained from genetic and biochemical studies in yeast. Interestingly, somatic mutations in eIF1A, especially in the NTT, were recently found to be associated with uveal, thyroid and ovarian cancers (6-9). Combination of eIF1A and Ras mutations has been reported in different types of epithelial cancer (Thyroid Carcinoma) and melanomas (7, 8). Presently very little is known about the biological function of eIF1A in mammalian cells and how perturbations of this function contribute to cancer.

In the present study we used mammalian cells to investigate the physiological and molecular functions of eIF1A and how eIF1A-NTT cancer-associated mutants alter these activities. We report that eIF1A has a critical role in maintaining cell proliferation and cell cycle progression by supporting the G2/M phase of the cell cycle. Using ribosome profiling to explore the translational landscape of cells depleted of the two eIF1A paralogs, we find 2 major subsets of eIF1A-regulated mRNAs, both of which are related to the function of eIF1A-CTT. The downregulated gene set is enriched with cell cycle genes and predominantly characterized by lengthy 5'UTR thus dependent on the scanning promoting activity of eIF1A-CTT. The other gene class display dramatic stimulation of initiation in 5'UTRs at near-cognate AUG codons which is unexpectedly linked to translation upregulation, most likely via reinitiation. This observation uncovers those mRNAs that are targeted by eIF1A for

suppression of inappropriate initiation. We further demonstrate that the cancer-associated NTT mutants elevate the scanning promoting activity eIF1A on long 5'UTR but have little effect on AUG selection. At the molecular level, these mutations diminish eIF1A interaction with A-site ribosomal proteins Rps3 and Rps10 which are involved in scanning arrest. Our findings provide a mechanistic basis for promotion of cell proliferation by eIF1A-NTT mutants which involves scanning enhancement of long 5'UTR-containing cell cycle genes.

Results

eIF1A is essential for cell proliferation and cell cycle progression

To address the function of eIF1A we initially attempted to knockout the two paralogs of eIF1A encoded by chromosomes 18 [eIF1A(18)] and X (eIF1AX) that are expressed in mouse embryonic fibroblasts (MEFs) using CRISPR-Cas9 system. However, we could not obtain stable double knockout of these paralogs. We therefore used siRNA against the two eIF1A encoding genes which resulted in efficient downregulation of eIF1A mRNAs and protein (Fig. 1A). eIF1A KD caused a visible effect on cell number (Fig. 1B) which was validated by live-cell counting (Fig. 1C) and a luminescent cell proliferation assay (Fig. 1D), suggesting that it is required to maintain cell proliferation.

To investigate whether the reduced cell number seen upon eIF1A depletion is associated with alterations in the cell cycle, we analyzed the partition of cells in G1, S and G2/M phases of the cell cycle by flow cytometry following DNA staining with propidium iodide. The results revealed that eIF1A KD caused substantial changes in the distribution of cells at the different phases of the cell cycle. Specifically, we observed in eIF1A KD accumulation of cells in the S phase along with a dramatic decrease in cells of G2/M phase of the cell cycle compared with control (Fig. 1E). In addition, there is an increase in the sub-G1 dead cells in the eIF1A KD cells. These results suggest that the growth defect associated with eIF1A depletion can be attributed to a block in S phase or impaired transition from S to G2/M along with reduced cell survival. Thus, the two eIF1A genes are most likely essential for cell proliferation and survival in MEFs which can explain the unsuccessful attempts to knock them out.

eIF1A depletion causes extensive changes in translation of cell cycle genes

To examine the impact of eIF1A on translation, MEFs were transfected with control or combination of eIF1AX and eIF1A(18) siRNAs for 72 hours (eIF1A KD) and then lysed and subjected to sucrose gradient sedimentation. The polysome profile of eIF1A depleted MEFs was dramatically changed compared to control, as the relative amount of 80S monoribosome was increased while polysomal fractions were substantially decreased (Fig. S1), indicating for inhibition of translation. To study further the changes in translation initiation landscape of eIF1A KD cells we applied the ribosome profiling (RP) approach in the presence of harringtonine (Hrr) and cycloheximide (CHX) as translational inhibitors as described previously (10). We performed deep sequencing of the ribosomal protected RNA fragments along with mRNA-seq of control and eIF1A depleted MEFs. Analysis of the length of the ribosome-protected fragments revealed the expected 28-31-nucleotide peaks in all samples (Fig. 2A) and comparison of the two biological repeats using scatter plot indicate for their high similarity (Fig. 2B). Inspection of the read coverage of eIF1AX and eIF1A(18) genes confirmed efficient knockdown of the two paralogs at the mRNA and translation levels (Fig. S2). Meta-gene analysis of the distribution of normalized reads in the coding region (CDS) of 6331 genes revealed that the overall coverage of the two eIF1A KD samples is generally lower than that of control samples (Fig. 2D, left). Considering the expected general role of eIF1A, it was surprising that its depletion resulted in CDS translational down regulation of only 1014 and upregulation of 439 genes (Fig. 2C) while the vast majority of mRNAs were unaffected. Meta-profiles of the downregulated gene set revealed reduced ribosome occupancy, particularly in the mRNAs bodies, in the two KD samples compared to their controls (Fig. 2D, right). This finding is consistent with the reduction in the amount of polysomes seen in the polysome

profiling following eIF1A KD (Fig. S1) which together suggest that eIF1A depletion causes a defect in the transition from initiation to elongation in this subset of genes.

The translation of TOP-containing mRNAs that include ribosomal proteins and translation initiation factors, is known to be effectively downregulated in response to a variety of stresses (11, 12). The RP data revealed that neither ribosomal proteins nor translation initiation factors are among the translationally downregulated genes (Table S1). We confirmed this observation by analyzing the levels of a subset of these proteins to which antibodies were available and found them to be largely unchanged (Fig. S3). Likewise, the translation of several mRNAs known to be up-regulated in response to stresses that elevate eIF2 α serine 51 phosphorylation such as ATF4 and CHOP (DDIT3), were unaffected by eIF1A KD (Table S2). These findings rule out the possibility that the translational effect seen upon eIF1A depletion is indirectly related to translational stress-response.

Biological pathway analysis indicate that the most enriched categories associated with the downregulated gene set are related to cell cycle and include cell cycle, DNA damage response and repair, mitotic cell division and G2/M transition of mitotic cell cycle (Fig. 2E). Translational downregulation of these categories can explain the observed cell proliferation and cell cycle progression defects associated with eIF1A KD (Fig. 1E). Examples of several translationally downregulated cell cycle genes that include Wee1, Tgfb1, Nedd1, Rad21 Usp8 and Khlh9 can be seen in Fig. 3. The ribosome occupancy in the CDS of all these representative genes is substantially reduced. Analysis of several proteins from these pathways by western blot confirms that their diminished translation upon eIF1A KD leads to reduced protein levels (Fig. 2G). Analysis of the downregulated genes in a disease database revealed enrichment of various types of cancers more than any other disease (Fig. 2F), highlighting the importance of eIF1A in this pathology.

Translational control by eIF1A is largely determined by the 5'UTR length

Considering the role that eIF1A plays in the stringency of start codon selection (13) we compared the context of the start codon of the eIF1A-dependent mRNAs to the AUG flanking sequence of the unaffected mRNAs. As can be seen in Fig. 4A the logos of the downregulated, upregulated and unaffected gene sets are almost indistinguishable. Thus, the requirement of eIF1A for the downregulated mRNAs seems to be largely AUG-context-independent. Next, we compared the 5'UTR length between the different gene sets and found that the downregulated and upregulated mRNAs are significantly longer and shorter, respectively, compared to the unaffected genes (Fig. 4B). To examine whether the 5'UTR length is relevant to the eIF1A-dependent cell-cycle genes, which constitute only 8% of all the downregulated genes, we specifically analyzed the 5'UTR size and found that they have indeed longer 5'UTR compared to the unaffected or upregulated gene sets (Fig. 4B).

To investigate further the association of 5'UTR length and eIF1A regulation we used two reporter genes which have identical strong AUG context but differ in their 5'UTR length as shown schematically in Fig. 4C. MEFs were transfected with control or eIF1AX plus eIF1A(18) siRNAs and 48h later transfected again with these siRNAs together with the two reporters. The results, which are expressed as the ratio between the long (Renilla) and the short (Firefly) luciferase activities, revealed diminished relative activity of the long 5'UTR in eIF1A KD cells compared to control (Fig. 4D). The observed effect is not a consequence of differential expression of the short and long mRNAs in eIF1A KD cells (Fig. 4E). Thus, the ribosomal profiling along with the reporter gene assays suggest that 5'UTR length is the primary feature involved in the translational control by eIF1A in mammalian cells.

Marked increase in 5'UTR translation initiation in response to eIF1A KD

We next analyzed relative levels ribosomal occupancies in the 5'UTR and we observed that there is an overall increase in 5'UTR ribosomal footprints upon eIF1A KD. Specifically, 1907 expressed genes, that constitute 28% of all analyzed genes show upregulation of >2-fold in their 5'UTR (Fig. 5A). This effect is clearly evident from the meta-gene profile of all genes (Fig. 5B, left) and of this gene set (Fig. 5B, right). As uORF can have important regulatory role on translation of the main ORF (14, 15), we compared the 5'UTR up-regulated gene set to the genes displaying down and up regulation of translation in their CDS using Venn diagram (Fig. 5C). Interestingly, there is very little overlap between the genes displaying enhanced 5'UTR footprints with the CDS downregulated genes, suggesting that elevated 5'UTR initiation does not significantly contribute to the regulation of these gene set by eIF1A. On the other hand, a substantial overlap is seen with the CDS upregulated gene set. Interestingly, the 5'UTR length of this specific overlapping set is significantly shorter than the rest of the 5'UTR upregulated set (Fig. S4), raising the possibility that increased 5'UTR translation contributes to enhanced CDS translation, most likely via re-initiation.

Translation initiation from the major ORF primarily occurs via AUG while initiation from 5'UTR tend to be more flexible and utilize near-cognate AUGs (16). We examined the sequence context of the translation initiation site (TIS) in the reads of the 5'UTR in control and eIF1A KD samples and found that the most variable nucleotide is the first of the AUG triplet (Fig. 5D). We also determined the percentage of all possible combinations of AUG single substitutions (Fig. 5E). The results confirm that the first nucleotide is the most diverged, but in the case of eIF1A KD 13% of the TISs occur in ACG triplet which is very rare in the control sample. Several specific examples that include Jun, Mrps17, Slc35e4 and Atp5g3 can be seen in Fig. 5F.

The features associated with the enhanced 5'UTR translation suggest that eIF1A depletion enhances the frequency of near-cognate AUG utilization in 5'UTRs. To examine this notion further, we used a series of luciferase reporter genes in which the initiating triplet is either AUG, CUG, GUG and UUG (Fig. 5G, top). Cells were depleted of eIF1AX plus eIF1A(18) using siRNAs and 48h later transfected again with these siRNAs together with the NUG reporters. The activities of CUG, GUG and UUG, which are expressed as percentage of AUG, were significantly enhanced by eIF1As KD (Fig. 5G). These findings provide strong support to the idea that eIF1A indeed acts to inhibit 5'UTR translation at near-cognate AUG in mammalian cells.

eIF1A is an essential component of eIF1 autoregulatory feedback loop

eIF1 plays a central role in scanning and AUG selection in an optimal context. eIF1 itself has an evolutionarily conserved poor AUG context that is necessary for an autoregulatory negative feedback loop in which high eIF1 levels inhibits its own translation and prevents its overexpression (17). Considering the overlapping functions of eIF1A-CTT and eIF1 we analyzed the effect of eIF1A depletion on eIF1 translation. Remarkably, we found that eIF1 translation is substantially upregulated (Fig. 6A). Consequently, eIF1 protein levels are dramatically elevated in eIF1A KD cells (Fig. 6B), suggesting that the autoregulatory negative feedback loop is severely disrupted. The mRNA levels of eIF1 are also increased (Fig. 6C), presumably due to the effect of translation on mRNA stability. We noticed that the elevation of eIF1 upon eIF1A depletion is associated with the appearance of translation initiation sites in the 5'UTR at CUG and ACG codons, which are hardly detected in control cells. Thus, eIF1 ability to restrict its own translation in the 5'UTR and the main ORF is lost in the absence of eIF1A. Considering the strong scanning-promoting activity of eIF1 (see for example (18, 19)),

one would expect translation of long 5'UTR mRNAs to be elevated due to this dramatic upregulation upon eIF1A KD. Contrary to this expectation long 5'UTR mRNAs are in fact downregulated (Fig. 4), suggesting that the scanning promoting activity of eIF1 requires its cooperation with eIF1A.

Cancer associated eIF1A NTT mutants primarily enhance translation of long 5'UTR mRNAs

Several studies revealed a link between somatic mutations in eIF1A, especially in the NTT, and cancers of uveal, thyroid and ovaries (6-9). Given the importance of eIF1A for the translational control of cell cycle genes via their long 5'UTR and the established role of cell cycle dysregulation in tumorigenesis, we set out to examine the function of cancer-associated NTT mutations. We used overexpression studies which bear some similarity with cancer cells in which eIF1A mutant co-exists with the WT proteins. MEFs were transfected with the long and short 5'UTR reporter genes described in Fig. 4C together with WT and mutant eIF1A plasmids (Fig. 7A). The results revealed that exogenous eIF1A enhanced the activity of the long 5'UTR reporter as compared to the short one (Fig. 7B). Interestingly, the effect of all the NTT mutants is significantly greater than that of the WT (Fig. 7B). Analysis of selected mutants in human HEK293T cells revealed similar enhancement of the long 5' UTR translation by NTT mutants compared to WT (Fig. 7C), confirming that this effect is not confined to a single cell type. To examine further the effect of eIF1A-NTT mutation on short and long 5'UTR mRNA we carried a polysomal profiling following a similar transfection experiment with eIF1A WT and G8R/G9R mutant together with short and long 5'UTR reporter genes. Both eIF1A variants cause a modest increase in the heavy polysomal fractions (Fig. 7D). Comparing the effects on short and long 5' UTR mRNAs revealed a clear differential enhancement of the long 5'UTR by G8R/G9R mutant (Fig. 7E and F). We also analyzed the effect of the WT and the NTT mutants

on CUG-driven translation but no significant effect was observed (Fig. S5). These findings suggest that the effect of these mutations is primarily related to 5'UTR length rather than initiation site stringency in mammalian cells.

NTT mutants are defective in A-site Rps10 and Rps3 binding

In the PIC eIF1A is located near A-site ribosomal proteins Rps3 and Rps10 and the mRNA channel (20). Both ribosomal proteins contact AUG downstream nucleotides and implicated in scanning arrest of short 5'UTR mRNAs bearing the TISU element (5). In addition, Rps3 and Rps10 were shown to interact with eIF1A in a cell-based split-Renilla assay (5). Considering the potential role of Rps3 and Rps10 in scanning inhibition we set to determine the impact of eIF1A NTT mutations on the binding to these ribosomal proteins. We first determined whether these interactions are direct using pull down assays. His-Rps3, His-Rps10 and eIF1A (tag-less) were each expressed in *E. coli*. His-Rps3 and His-Rps10 were incubated with nickel agarose beads in the absence or presence of eIF1A (Fig. 8A and B, lanes 3 and 5, respectively). As a control eIF1A was incubated with empty nickel beads (Fig. 8A and B, lane 4). The results revealed efficient binding of eIF1A to both ribosomal proteins (Fig. 8A and B, lane 5), confirming their direct specific interaction. Next, a similar analysis was carried with 3 eIF1A NTT mutants G6D, G9D/R13H (double mutant) and K10E (Fig. 8A, lanes 6-18 and Fig. 8B, lanes 6-16). Quantifying the relative amount of bound protein revealed a marked reduction in the amount of bound K10E mutant on RPS3 as compared to WT while the effect of the binding to Rps3 by G6D and G9D/R13H mutants was not significant (Fig. 8A&C). With Rps10 all mutants G6D, G9D/R13H and K10E bound less efficiently. Thus, it can be concluded that at least part of the effect of the eIF1A NTT mutations on translation may be attributed to reduced binding to ribosomal proteins.

Discussion

In this study we addressed the biological function of eIF1A and the mechanism underlying the translational dysregulation conferred by eIF1A-NTT mutations in mammalian cells. By downregulating the two eIF1A paralogs in MEFs we demonstrate a critical role of this factor in promoting **cell proliferation** and cell cycle progression with a particular defect in G2/M phase of the cell cycle. Exploring the translation landscape of cells depleted of both eIF1A paralogs using ribosome profiling, we uncovered 2 major non-overlapping subsets of eIF1A-regulated mRNAs, which are related to known molecular attributes of eIF1A. The first includes 1014 mRNAs displaying translation downregulation of the major ORF. This set is highly enriched with cell cycle as well as cancer associated genes indicating that eIF1A plays a critical role in driving translation of these mRNAs and highlighting the potential contribution of its deregulation to cancer. Considering the importance of this factor in initiation site selection based on the stringency of the AUG context (2, 4), it was unexpected to observe that the most specific feature characterizing this gene set is lengthy 5'UTR rather than differences in the AUG context, a finding that was also validated by reporter gene assay. This observation raises the possibility that maintaining the stringency of AUG context in ORFs is fulfilled by other initiation factors with similar activity. Thus, in the downregulated gene set the most important function conferred by eIF1A is the facilitation of scanning, an activity known to be mediated by the scanning enhancer present in eIF1A-CTT. On the other hand, eIF1A-NTT was shown to bear a scanning inhibitor (21). As all the 7 cancer-associated eIF1A-NTT mutants analyzed here displayed higher scanning promoting activity compared to WT, it can be concluded that these mutants are defective in scanning inhibition. Thus, it is likely that cancer cells benefit from eIF1A's ability to enhance scanning to facilitate translation of cell cycle and tumor promoter genes such as those identified here.

The largest gene collection affected by eIF1A depletion is characterized by elevated translation initiation in 5'UTR at near cognate AUG, suggesting for relaxation of start codon stringency and higher frequency of scanning-arrest at these sites (ribosomal closed confirmation). This is clearly exemplified by the dramatic increase in the utilization of the ACG triplet as a start codon in the eIF1A KD samples and the results with the NUG reporter gene assay which demonstrate heightened near-cognate AUG initiation upon eIF1A depletion. Thus, it appears that eIF1A has a major role in preventing initiation from near cognate AUG in the 5'UTRs of mammalian genes, to maintain protein homeostasis and avoid energy expenditure. As this inhibitory activity is also attributed to the CTT of eIF1A, it seems that this domain is dominant relative to the NTT in mammalian cells.

Remarkably, 55% of those mRNAs that present elevated translation in the main ORF overlap with the mRNAs displaying increased 5'UTR translation (Fig. 5C), suggesting for a functional link between these effects. This observation was unexpected as uORF tend to diminish translation from a downstream main ORF (14, 15). One possibility that can explain this link is the process of translation reinitiation, a mechanism in which an uORF can retain the small ribosomal subunit on the mRNA after termination and initiate translation at a downstream site as occurs in stress response mRNAs such as the yeast GCN4 and its mammalian homolog ATF4 (22-24). Reinitiation efficiency depends on several features and factors, of which a major one is the distance of the uORF from the main ORF. A hint that this mechanism may indeed be involved in the translation up-regulation here is the fact that this set is generally characterized by shorter 5'UTR length and therefore increased likelihood for a short distance between the uORF and the main ORF. Thus, inhibition of 5'UTR initiation by eIF1A not only serves to prevent wasteful uORF synthesis but also to keep the translation of

mRNAs with relatively short 5'UTR under control. Interestingly, in mammalian cells the eIF1A-NTT mutants do not show enhanced inhibition of near-cognate AUG selection compared to WT eIF1A (Fig. S5), whereas these mutations in yeast eIF1A enhance the stringency of initiation site selection (25). This finding can be explained by a higher degree of redundancy of this activity among mammalian eIFs as well as the fact that both eIF1 and eIF1A are each encoded by at least two genes.

The genes encoding eIF1 in most eukaryotes contain an AUG in a poor context (17, 26) and eIF1 itself inhibits translation from AUG context that diverges significantly from the Kozak (18, 27). Consequently it was found that mammalian eIF1 negatively autoregulates its own translation in a manner that is dependent on the poor context of its start codon (17). Thus, eIF1 cannot be overexpressed in cells. Interestingly, our findings revealed that this autoregulatory loop is severely disrupted upon loss of eIF1A, as eIF1 translation is dramatically elevated and eIF1 protein levels rise substantially. This finding uncovered the important role of eIF1A in limiting eIF1 translation and the cooperation of these factors in discriminating against poor AUG context. Furthermore, despite the dramatic eIF1 upregulation upon eIF1A KD, the mRNAs that are downregulated tend to have longer 5'UTR, suggesting that eIF1 cannot compensate for eIF1A loss and most likely their ability to promote scanning is interconnected.

The cryo-EM structure of the 48S in the presence of eIF1 and eIF1A suggest that eIF1A is located near the A-site and the mRNA channel around +4 and +5 positions and is also in proximity to the 18S rRNA, RPS3 and RPS10 (20). Here we show that eIF1A interacts directly with each Rps3 and Rps10 and that both interactions are weakened by several cancer-associated NTT mutants. The effects of these mutations on binding to mRNA and 18S are yet

to be determined. As these mutants also impair the scanning inhibition associated with this domain, we infer that eIF1A-Rps3/10 interactions serve to promote scanning arrest and the 'closed' conformation. These findings nicely fit our recent report of the involvement of Rps3 and Rps10 in the scanning arrest promoted by TISU, a translation regulatory element that directs cap-dependent and scanning-free initiation (18, 19, 28). Both Rps3 and Rps10 were specifically cross-linked to positions +5 and + 6 of TISU in a dynamic manner (5). In this study TISU was also found to be highly dependent on eIF1A. It was therefore unexpected that TISU genes were not found to be enriched among the eIF1A affected genes. A possible explanation for this may be related to the dramatic upregulation of eIF1 upon eIF1A KD in MEFs. As TISU activity is highly eIF1 dependent and eIF1 was shown to compensate for the absence of eIF1A in *in vitro* translation assays (19) it is possible that eIF1 and eIF1A also play redundant regulatory role in TISU-mediated translation in MEFs. An alternative explanation may relate to the short 5'UTR length of TISU mRNAs which may result in a footprint at the initiation site that has shorter length than 28 nt.

In summary, by combining global translation analysis of cells depleted of the two eIF1A paralogs along with complementary studies of the cancer associated mutants of eIF1A, we uncovered the most important mRNA features underlying differential regulation of distinct mRNAs by eIF1A in mammalian cells. In particular, our findings point to the essential function of eIF1A-CTT which has fundamental and non-redundant role in promoting scanning of long 5'UTR mRNAs and inhibiting inappropriate 5'UTR translation. Thus eIF1A-CTT emerges as a potential target for drugs against cancers with and without eIF1A mutations.

Materials and Methods

eIF1A knockdown experiments

Mouse embryonic fibroblasts were transfected using RNAimax lipofectamine (Cat no. 13778075) with either 50 nM control siRNA (Non-targeting Control siRNAs: D-001810-03-20, Dharmacon, GE Healthcare life sciences), or siRNAs targeting chromosome 18 eIF1A (SMARTpool: D-0625552-01) and si-eIF1AX, (SMARTpool: D-063045-01) both from Dharmacon, GE Healthcare life sciences. The SMARTpool consists of 4 distinct siRNAs for each gene. 24h later cells were split and after additional 24h were transfected again with the siRNAs. 72h after the initial transfection, cells were harvested for the various analyses described in the results section.

Cell viability experiments

MEFs in a 6-well plate were transfected with control or eIF1A siRNAs as described above. After 72h, cells were subjected to cell viability measurement using CellTiter-Glo Luminescent Assay (Cat no. G7571, Promega). In addition, eIF1A knockdown and control cells were stained with trypan blue (cat no. T8154, Sigma) and live cells were counted using Biorad TC20 cell counter.

Cell cycle analysis

MEFs were transfected with control or eIF1A siRNA as described above. eIF1A KD and control MEFs were trypsinized and washed twice with ice cold PBS. Subsequently, cells were fixed overnight in 70% ethanol and washed twice with ice cold PBS and resuspended in staining buffer (0.1% triton X-100, 2mg RNase A and 4% propidium iodide), and incubated at 37°C for

15 minutes. Cells were monitored by BC LSRII flow cytometer and data was analyzed using Modfit Lt Software.

Ribosome profiling

Ribosomal footprinting were generated essentially as described in MEFs (10). Briefly, MEFs in 10 cm plates were transfected with control or eIF1A siRNA as described above. 72h later cells were incubated with 2µg/ml harringtonin (HR) (LKT Laboratories, cat.no. H0169) for 2 minutes followed by addition of 100µg/ml cyclohexamide (CHX). Cells were lysed and were used for ribosomal footprinting and library preparation as described (10) and for total RNA preparation. The resulting ribosome profiling libraries were sequenced on HiSeq2500 High-Output instrument (Illumina) to yield 60 bp single-end reads. RNA-seq was performed using derivation of MARS-seq as described (29). The final mRNA libraries were sequenced using high-throughput 75 bp kit (Illumina FC404-2005) on NEXTseq 500 instrument to yield 75 bp paired end reads.

Data analysis of the ribosome profiling

Preprocessing and alignment - The number of input RP reads per sample was in the range of 52M -62M single end of length 61 bases. Initial analysis steps are similar to described in Ingolia et al. (10) and consisted of preprocessing sequences by removing first base and adapter and filtering for sequences of length 20 to 50 with cutadapt (<http://journal.embnnet.org/index.php/embnnetjournal/article/view/200/479>; parameters : -a CTGTAGGCACCATCAATAGATCGGAAGAGCACACGTCTGAACTCCAGTCAC --discard-untrimmed --times 1 -u 1 -m 20 -M 50) in other words keeping sequences that had adapter (not trimming by quality of bases). rRNA was removed by running bowtie (30) against a database of rRNA

downloaded from <http://genome.ucsc.edu/cgi-bin/hgTables> and making a fastq file of non-rRNA sequences (bowtie parameters: -norc -un). The number of reads remaining was in the range 24M-30M. Next, sequences were aligned to refSeq mm10 transcripts (downloaded from iGenomes) using bowtie (parameters --norc -S -l 25 -n 2 -m 100 --best --strata). Proportion plots of aligned reads to length of reads was done using riboSeqR package (Bioconductor) after converting the sam file to bam with samtools (31). For gene quantification and RP summit detection, reads of length 28-33 were selected using cutadapt (parameters: -m 28 -M 33) and aligned to mm10 mouse genome using TopHat2(32) (parameters : --no-novel-juncs --library-type fr-firststrand). Bam files were converted to tdf files using igvtools count, in order to view with IGV(33). Number of reads aligned were in the range 3.5M-5M, out of them more than half aligned uniquely.

CDS and 5'UTR quantification - For quantification UTR and CDS gtf files were created from refseq annotation, avoiding regions found in both region types. HTSeq was used for the quantification (parameters -s yes -t exon -m intersection-nonempty). The option intersection-nonempty allows to assign junction reads to either the CDS or UTR, depending where most of the read is placed. The number of reads quantified as 5' UTR range from 107K to 135K and to CDS range from 270K to 808K.

Translation efficiency, 5'UTR length and start codon analyses - Counts for 5' UTR and CDS were unified per sample and the quartile distribution was calculated. Since 75% of the counts were below 26, only genes that had at least 26 counts in one of the samples were used in subsequent steps. Variations in sample sizes were normalized using the DEseq2 statistical R language package(34). Translation efficiency for each sample was calculated from the ratio of ribosome profiling counts compared to Mars-seq mRNA levels for 5' UTR and CDS separately. Thereupon, the ratio between samples and controls was calculated on log

transformed data. Genes were categorized into upregulated or downregulated if the sample vs control ratio of translation efficiency was over 1 or under -1 for both samples, respectively, or unaffected for all other cases. The mean 5' UTR length (for all transcripts defined in the iGenomes Illumina mm10 gtf file) per gene distribution was calculated for the aforementioned categories. Differences between gene categories was evaluated using one-way ANOVA and effect size was estimated using Cohen's D. Cell cycle genes, which represent a subset of genes that are downregulated in their CDS translation efficiency ratio, were separately compared to upregulated or unaffected genes. Similarly, mean 5' UTR length distribution was also performed for categories in a pairwise fashion after mutually excluding genes that belong to both categories (intersection).

Start codon boundary (± 6 bp) sequences were retrieved from a fasta file containing all mm10 mRNA sequences (downloaded from the NCBI nucleotide page search using "mouse[organism]" and filtered for mRNA and refseq using the left panel) using the bedtools getfasta program. Thereupon, logos were created using MEME (-minw 6 -maxw 9 -maxsize 1000000 -rna)(35)

Finding Ribosome profiling summits in 5'UTR - Regions enriched with RP within 5'UTR were identified using macs (36) (parameters: -g 3e9 --keep-dup all --nomodel --shiftsize=1) with no model and no filtering of PCR duplicates. Summit peaks were annotated by intersection (intersectBed (37)) with refSeq gtf file, shifted 12 bases and expanded to 3 bases (awk commands). Bed files were derived for peaks appearing on both replicates and are within 5-UTR the region and can be extended to 9 bases within exon 5'-UTR boundaries (IntersectBed and a Perl script). These peaks bed files were divided according to gene lists (TE down UTR, TE up UTR and TE unaffected) (dedicated perl script) and their sequence was extracted to

fasta files (bedtools getfasta). Motif enrichment search within 5' UTR ribosome profiling extended summit sequences was done with MEME (35) (parameters: -minw 6 -maxw 9 -rna). *5'UTR and CDS body coverage plots* - Used RSeQC (38) geneBody_coverage.py script to plot the coverage using the Tophat bam and 5'-UTR and CDS regions bed12 format (long bed) files. A perl script was used to create bed files for the specific gene lists (need to match transcript name to gene and extract the relevant genes bed file).

Plasmids

To generate eIF1A expression plasmids the eIF1AX cDNA was isolated by RT-PCR from HEK293T RNA and then cloned in pCDNA3 via BamHI and XhoI sites. The seven eIF1A mutants (G6D, G9D, G9R, G8RG9R, K10E, R13H and G15D) were generated by site directed mutagenesis using Q5® Site-Directed Mutagenesis Kit from New England BioLabs. The NUG firefly luciferase and Renilla luciferase plasmids were kindly provided by Prof. Kastura Asano (Kansas State University). The short and the long 5' UTRs of the firefly and Renilla luciferase are derived from SV40.

Binding Assay

eIF1A-WT and mutants (G6D, G9D/R13H and K10E), His tagged Rps3 and His tagged Rps10 were each cloned in pRSFDuet-1 vector. The respective protein was expressed using BL-21 expression system. Binding assay was performed using Ni-NTA His-bind Resins (Novagen) followed by western blot. Western blots were quantified using Image studio lite ver 5.2.

Acknowledgements

This work was supported by grants from the Minerva Foundation (#712278), Israel Science Foundation (#843/17) and an internal grant donated by Auctoriana Anstalt organization. R.D. is the incumbent of the Ruth and Leonard Simon Chair of Cancer Research.

Author Contributions

R.D and U.S conceived and designed the study, analyzed the data and wrote the paper. U.S. carried out most of the experiments; F.K. and S.A. performed part of the experiments; G.Z. and D.L. performed the analysis of the ribosomal profiling data.

Conflict of Interest

The authors declare that they have no conflict of interest.

References

1. **Chu J, Cargnello M, Topisirovic I, Pelletier J.** 2016. Translation Initiation Factors: Reprogramming Protein Synthesis in Cancer. *Trends Cell Biol* **26**:918-933.
2. **Hershey JW, Sonenberg N, Mathews MB.** 2012. Principles of translational control: an overview. *Cold Spring Harb Perspect Biol* **4**.
3. **Hinnebusch AG.** 2014. The scanning mechanism of eukaryotic translation initiation. *Annu Rev Biochem* **83**:779-812.
4. **Hinnebusch AG, Lorsch JR.** 2012. The mechanism of eukaryotic translation initiation: new insights and challenges. *Cold Spring Harb Perspect Biol* **4**.
5. **Haimov O, Sinvani H, Martin F, Ulitsky I, Emmanuel R, Tamarkin-Ben-Harush A, Vardy A, Dikstein R.** 2017. Efficient and Accurate Translation Initiation Directed by TISU Involves RPS3 and RPS10e Binding and Differential Eukaryotic Initiation Factor 1A Regulation. *Mol Cell Biol* **37**.
6. **Ewens KG, Kanetsky PA, Richards-Yutz J, Purrazzella J, Shields CL, Ganguly T, Ganguly A.** 2014. Chromosome 3 status combined with BAP1 and EIF1AX mutation profiles are associated with metastasis in uveal melanoma. *Invest Ophthalmol Vis Sci* **55**:5160-5167.
7. **Karunamurthy A, Panebianco F, S JH, Vorhauer J, Nikiforova MN, Chiosea S, Nikiforov YE.** 2016. Prevalence and phenotypic correlations of EIF1AX mutations in thyroid nodules. *Endocr Relat Cancer* **23**:295-301.
8. **Etemadmoghadam D, Azar WJ, Lei Y, Moujaber T, Garsed DW, Kennedy CJ, Fereday S, Mitchell C, Chiew YE, Hendley J, Sharma R, Harnett PR, Li J, Christie EL, Patch AM, George J, Au-Yeung G, Mir Arnau G, Holloway TP, Semple T, Pearson JV, Waddell N, Grimmond SM, Kobel M, Rizos H, Lomakin IB, Bowtell DDL, deFazio A, Australian Ovarian Cancer Study G.** 2017. EIF1AX and NRAS Mutations Co-occur and Cooperate in Low-Grade Serous Ovarian Carcinomas. *Cancer Res* **77**:4268-4278.
9. **Hunter SM, Anglesio MS, Ryland GL, Sharma R, Chiew YE, Rowley SM, Doyle MA, Li J, Gilks CB, Moss P, Allan PE, Stephens AN, Huntsman DG, deFazio A, Bowtell DD, Australian Ovarian Cancer Study G, Gorringer KL, Campbell IG.** 2015. Molecular profiling of low grade serous ovarian tumours identifies novel candidate driver genes. *Oncotarget* **6**:37663-37677.
10. **Ingolia NT, Brar GA, Rouskin S, McGeachy AM, Weissman JS.** 2012. The ribosome profiling strategy for monitoring translation in vivo by deep sequencing of ribosome-protected mRNA fragments. *Nat Protoc* **7**:1534-1550.
11. **Meyuhas O.** 2000. Synthesis of the translational apparatus is regulated at the translational level. *Eur J Biochem* **267**:6321-6330.
12. **Meyuhas O, Kahan T.** 2015. The race to decipher the top secrets of TOP mRNAs. *Biochim Biophys Acta* **1849**:801-811.
13. **Mitchell SF, Lorsch JR.** 2008. Should I stay or should I go? Eukaryotic translation initiation factors 1 and 1A control start codon recognition. *J Biol Chem* **283**:27345-27349.
14. **Tamarkin-Ben-Harush A, Schechtman E, Dikstein R.** 2014. Co-occurrence of transcription and translation gene regulatory features underlies coordinated mRNA and protein synthesis. *BMC Genomics* **15**:688.

15. **Calvo SE, Pagliarini DJ, Mootha VK.** 2009. Upstream open reading frames cause widespread reduction of protein expression and are polymorphic among humans. *Proc Natl Acad Sci U S A* **106**:7507-7512.
16. **Hinnebusch AG, Ivanov IP, Sonenberg N.** 2016. Translational control by 5'-untranslated regions of eukaryotic mRNAs. *Science* **352**:1413-1416.
17. **Ivanov IP, Loughran G, Sachs MS, Atkins JF.** 2010. Initiation context modulates autoregulation of eukaryotic translation initiation factor 1 (eIF1). *Proc Natl Acad Sci U S A* **107**:18056-18060.
18. **Elfakess R, Sinvani H, Haimov O, Svitkin Y, Sonenberg N, Dikstein R.** 2011. Unique translation initiation of mRNAs-containing TISU element. *Nucleic Acids Res* **39**:7598-7609.
19. **Sinvani H, Haimov O, Svitkin Y, Sonenberg N, Tamarkin-Ben-Harush A, Viollet B, Dikstein R.** 2015. Translational tolerance of mitochondrial genes to metabolic energy stress involves TISU and eIF1-eIF4GI cooperation in start codon selection. *Cell Metab* **21**:479-492.
20. **Hussain T, Llacer JL, Fernandez IS, Munoz A, Martin-Marcos P, Savva CG, Lorsch JR, Hinnebusch AG, Ramakrishnan V.** 2014. Structural changes enable start codon recognition by the eukaryotic translation initiation complex. *Cell* **159**:597-607.
21. **Saini AK, Nanda JS, Lorsch JR, Hinnebusch AG.** 2010. Regulatory elements in eIF1A control the fidelity of start codon selection by modulating tRNA(i)(Met) binding to the ribosome. *Genes Dev* **24**:97-110.
22. **Hinnebusch AG.** 2005. Translational regulation of GCN4 and the general amino acid control of yeast. *Annu Rev Microbiol* **59**:407-450.
23. **Kozak M.** 2001. Constraints on reinitiation of translation in mammals. *Nucleic Acids Res* **29**:5226-5232.
24. **Luukkonen BG, Tan W, Schwartz S.** 1995. Efficiency of reinitiation of translation on human immunodeficiency virus type 1 mRNAs is determined by the length of the upstream open reading frame and by intercistronic distance. *J Virol* **69**:4086-4094.
25. **Martin-Marcos P, Zhou F, Karunasiri C, Zhang F, Dong J, Nanda J, Kulkarni SD, Sen ND, Tamame M, Zeschnigk M, Lorsch JR, Hinnebusch AG.** 2017. eIF1A residues implicated in cancer stabilize translation preinitiation complexes and favor suboptimal initiation sites in yeast. *Elife* **6**.
26. **Miyasaka H, Endo S, Shimizu H.** 2010. Eukaryotic translation initiation factor 1 (eIF1), the inspector of good AUG context for translation initiation, has an extremely bad AUG context. *J Biosci Bioeng* **109**:635-637.
27. **Pestova TV, Kolupaeva VG.** 2002. The roles of individual eukaryotic translation initiation factors in ribosomal scanning and initiation codon selection. *Genes Dev* **16**:2906-2922.
28. **Elfakess R, Dikstein R.** 2008. A translation initiation element specific to mRNAs with very short 5'UTR that also regulates transcription. *PLoS ONE* **3**:e3094.
29. **Jaitin DA, Kenigsberg E, Keren-Shaul H, Elefant N, Paul F, Zaretsky I, Mildner A, Cohen N, Jung S, Tanay A, Amit I.** 2014. Massively parallel single-cell RNA-seq for marker-free decomposition of tissues into cell types. *Science* **343**:776-779.
30. **Langmead B, Trapnell C, Pop M, Salzberg SL.** 2009. Ultrafast and memory-efficient alignment of short DNA sequences to the human genome. *Genome Biol* **10**:R25.

31. **Li H, Handsaker B, Wysoker A, Fennell T, Ruan J, Homer N, Marth G, Abecasis G, Durbin R, Genome Project Data Processing S.** 2009. The Sequence Alignment/Map format and SAMtools. *Bioinformatics* **25**:2078-2079.
32. **Kim D, Pertea G, Trapnell C, Pimentel H, Kelley R, Salzberg SL.** 2013. TopHat2: accurate alignment of transcriptomes in the presence of insertions, deletions and gene fusions. *Genome Biol* **14**:R36.
33. **Thorvaldsdottir H, Robinson JT, Mesirov JP.** 2013. Integrative Genomics Viewer (IGV): high-performance genomics data visualization and exploration. *Brief Bioinform* **14**:178-192.
34. **Love MI, Huber W, Anders S.** 2014. Moderated estimation of fold change and dispersion for RNA-seq data with DESeq2. *Genome Biol* **15**:550.
35. **Bailey TL, Boden M, Buske FA, Frith M, Grant CE, Clementi L, Ren J, Li WW, Noble WS.** 2009. MEME SUITE: tools for motif discovery and searching. *Nucleic Acids Res* **37**:W202-208.
36. **Feng J, Liu T, Zhang Y.** 2011. Using MACS to identify peaks from ChIP-Seq data. *Curr Protoc Bioinformatics* **Chapter 2**:Unit 2.14.
37. **Quinlan AR, Hall IM.** 2010. BEDTools: a flexible suite of utilities for comparing genomic features. *Bioinformatics* **26**:841-842.
38. **Wang L, Wang S, Li W.** 2012. RSeQC: quality control of RNA-seq experiments. *Bioinformatics* **28**:2184-2185.

Figure legends

Figure 1: eIF1A is an essential for cell proliferation and cell cycle progression. **A.** Mouse embryonic fibroblasts (MEFs) were double transfected with Si-Control (non-targeting) or Si-eIF1A(18) plus Si-eIF1AX and 72h after the first transfection, RNA and protein lysates were prepared and subjected to real-time PCR western blot for measuring knockdown efficiency. The graph in the top panel shows the levels of eIF1A(18) and eIF1AX mRNAs normalized to GAPDH and the lower panel is immunoblot with eIF1A and tubulin antibodies as indicated. NC denotes negative control. **B.** Phase contrast microscope images showing cells transfected with Si-Control (left) and Si-eIF1A(18) plus Si-eIF1AX (right). The pictures were taken 72h after transfection. **C** and **D** represent cell viability of eIF1A KD and control MEFs was analyzed by trypan blue method and Luminescent Cell Viability Assay, respectively. **E.** Flow cytometric analysis of cell cycle using with propidium iodide DNA staining dye, of siControl MEFs (left) and si-eIF1A MEFs (right). The percentage of cells in the different phases of the cell cycle are indicated.

Figure 2: Ribosomal profiling of eIF1A KD cells reveals translation downregulation of cell cycle and cancer associated genes. **A.** Ribosome-protected fragment length (in nucleotides) in control and eIF1A KD samples (n=2 per sample category). **B.** Scatter plot shows the RPKM correlations ($R^2 > 0.9$) between the 2 independent replicate experiments of Control and eIF1A KD MEFs. **C.** A table summarizing the number of genes whose ribosomal occupancy was affected (fold change ≥ 2 or -2) or unaffected in coding regions (CDS) is response to eIF1A KD. **D.** Meta-gene analysis of the distribution of normalized reads in the coding region (CDS) of all analyzed gene (6331, left) and the downregulated genes (1014, right). **E.** Gene enrichment analysis of the biological processes associated with the CDS downregulated genes. The

number of genes in each category and the p -value are indicated. **F.** Gene enrichment analysis of diseases associated with the CDS downregulated gene. The number of genes in each category and the p -value are indicated. **G.** Western blot analysis of genes from the cell cycle and DNA repair categories that were translationally downregulated upon eIF1A KD. The levels of eIF1A and GAPDH (a control for unaffected gene) are also shown.

Figure 3: Consequences of eIF1A depletion on several cell cycle mRNAs. Tracks showing the ribosome profiling reads along various cell cycle mRNAs for replicate samples of each Control (green) and eIF1A KD (red). Blue bar denotes the actual translated coding sequence based upon ribosome profiling. Red arrow indicates direction of translation.

Figure 4. Translational control by eIF1A is predominantly determined by 5'UTR length. A. Analysis of the nucleotide context, using the MEME program, of the translation start site of the CDS unaffected, down and up gene sets. **B.** Box plot showing the relation between the 5'UTR length and translation efficiency of the CDS unaffected, down and up genes as well as the cell-cycle gene subset of the downregulated genes as indicated. The * denote statistically significant differences. **C.** Schematic diagram of the reporter gene constructs used to examine the role of eIF1A on 5'UTR length. The Renilla luciferase is preceded by a 5'UTR length of 311 nucleotides (upper) and the 5'UTR length of firefly luciferase is 111 nucleotides (lower). **D.** MEFs were transfected with control or eIF1AX plus eIF1A(18) siRNA and 48h later cells were co-transfected again with the siRNA pool together with the reporter genes described in C. Cells were harvested 24h after the second transfection and analyzed for Renilla and firefly luciferase activities. The graph presents the Renilla and firefly ratio of 6 independent experiments (average \pm SE). The * denote statistically significant differences, $p < 0.05$. **E.** The

effect of eIF1As KD on the mRNA levels of co-transfected reporter genes described in section C analyzed by RT-qPCR.

Figure 5. Broad elevation of 5'UTR initiation upon eIF1A depletion. **A.** The number of genes with the indicated alteration in 5'UTR translation upon eIF1A KD. **B.** Meta-gene analysis of the distribution of normalized reads in the 5'UTR region of all analyzed gene (6331, left) and upregulated genes (1907, right). **C.** Venn diagram showing overlap between CDS up, CDS down and 5'UTR up genes. **D.** Comparison of the nucleotide context of 5'UTR translation initiation site (TIS) in unaffected and upregulated genes. **E.** A pie chart showing the frequency (%) of start codon in the ribosome footprints in 5'UTR in the unaffected (right) and upregulated (left) gene sets. **F.** Tracks showing the ribosome profiling reads along various mRNAs with upregulation in ribosome density in 5'UTR for replicate samples of each Control (green) and eIF1A KD (red) samples. **G.** MEFs were transfected with control or eIF1AX plus eIF1A(18) siRNA and 48h later cells were co-transfected again with the siRNA pool together with a firefly luciferase reporter gene driven by AUG, CUG, GUG and UUG as a translation initiation codon as shown schematically on the top. Renilla reporter gene was also co-transfected and served as normalizing control. The activities of the NUG in control and eIF1A KD are presented as % of AUG of the indicated number of independent experiments (average \pm SE). The * denote statistically significant differences, $p < 0.05$.

Figure 6. eIF1A is a central player in eIF1 auto-regulatory feedback loop. **A.** Tracks showing the ribosome profiling reads along eIF1 mRNA for replicate samples of each Control (green) and eIF1A KD (red). **B.** eIF1 protein levels in control and eIF1A KD MEFs were analyzed by western blot along with eIF1A and GAPDH. This image is a representative of 3 independent

experiments with similar results. **C.** eIF1 mRNA levels in control and eIF1A KD MEFs derived from the RNA-seq data.

Figure 7. eIF1A NTT mutants primarily enhance translation of long 5'UTR mRNAs. A. Schematic view of eIF1A showing hotspot of NTT mutation reported in various carcinomas. **B.** Several of the eIF1A cancer-associated mutation were introduced in eIF1A expression plasmid. MEFs were transfected with the reporter genes described in Fig. 4C together with control or eIF1A WT and mutant expression plasmids. Cells were harvested 24h after transfection and analyzed for Renilla and firefly luciferase activities. The graph presents the Renilla (long 5'UTR) and firefly (short 5'UTR) luciferase activity ratio of the indicated number of experiments (average \pm SE). The * denote statistically significant differences, $p < 0.05$. **C.** The same experiment as in B with the indicated mutants was done in HEK293T cells. **D.** HEK293T were transfected with control, WT eIF1A and eIF1A G8R/G9R mutant plasmids together with the short and long 5'UTR reporter plasmids that are described in Fig. 4C. 48 hours after transfection cell lysates were subjected to sucrose gradient sedimentation and fraction collection to obtain the polysome profiles shown. **E.** Real-Time qPCR analysis of the indicated long (Renilla) and short (firefly) luciferase reporter mRNAs in the free, light and heavy polysomal fractions of the gradient of control, WT and mutant eIF1A expressing cells. **F.** The change in the polysomal to free ratio of the long and short mRNAs upon eIF1A WT and mutant expression calculated from the data of section E.

Figure 8. NTT mutants binding to Rps10 and Rps3 is defective. A&B. *In vitro* binding assays of eIF1A WT and mutants with Rps3 and Rps10. His tagged RPS3 (A) and His tagged RPS 10 (B) were coupled to Ni-agarose beads and incubated with un-tagged eIF1A WT or mutant as

indicated. As a control eIF1A was incubated with the Ni-agarose beads without Rps3/10. The pulled-down complexes were washed and then run on SDS-PAGE followed by western blot with the indicated antibodies. In all the experiments the input represents 2% of the amount of lysate used for the binding. **C.** Quantitation of the bound protein relative to the input. The graph represents the average \pm standard error (SE) binding level of 3 experiments. * denotes statistically significant difference ($p < 0.05$).

Figure 1

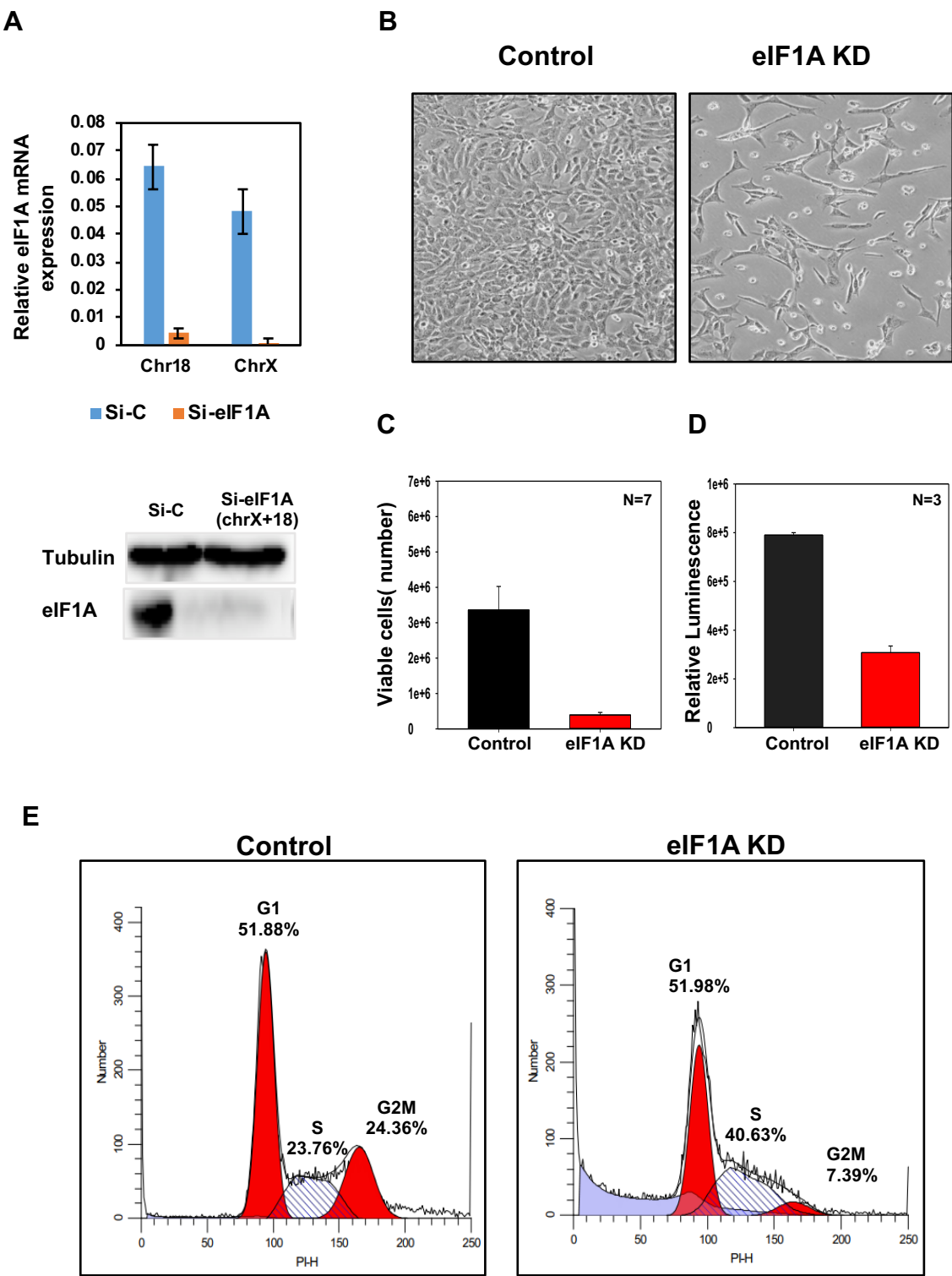


Figure 2

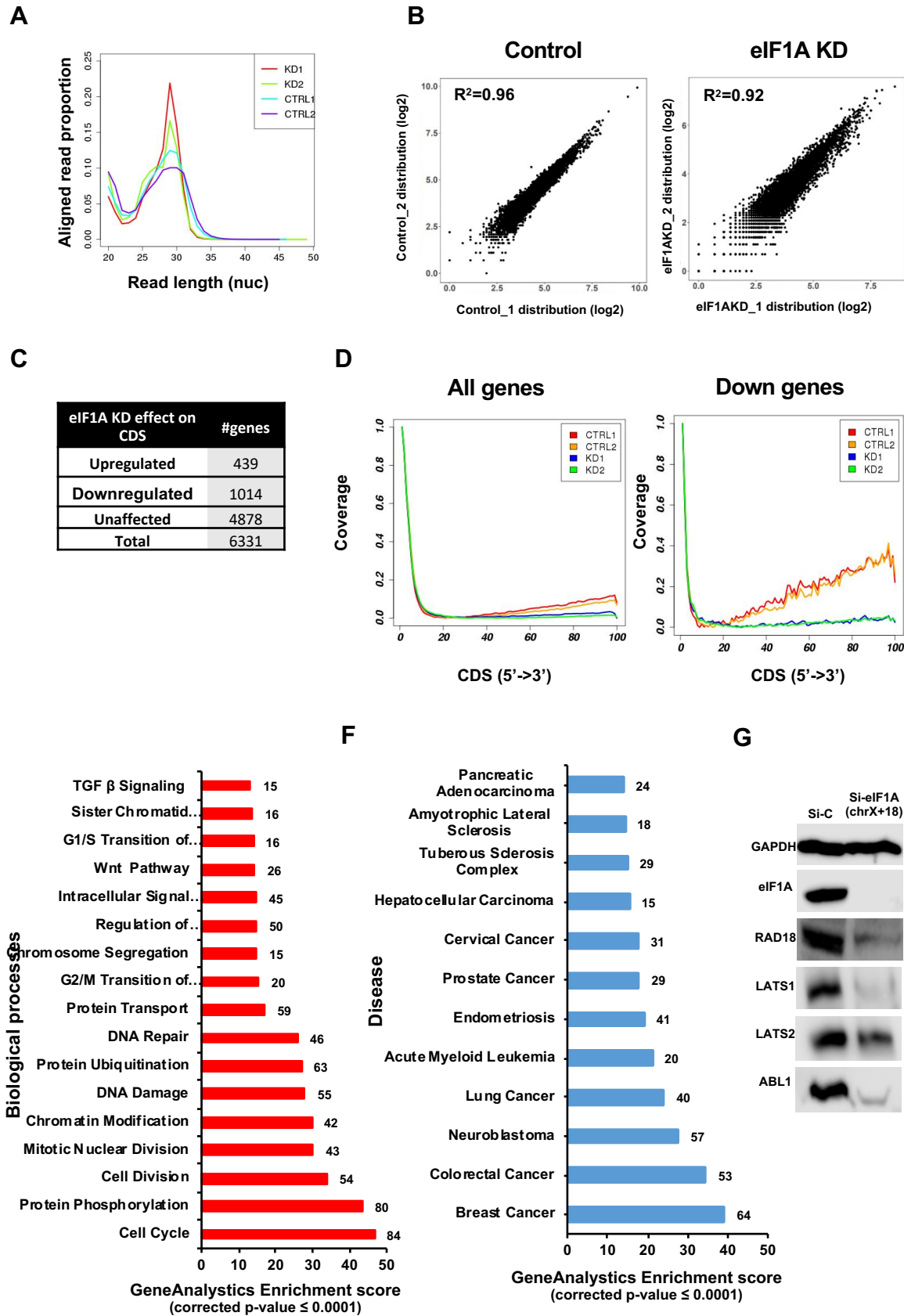


Figure 3

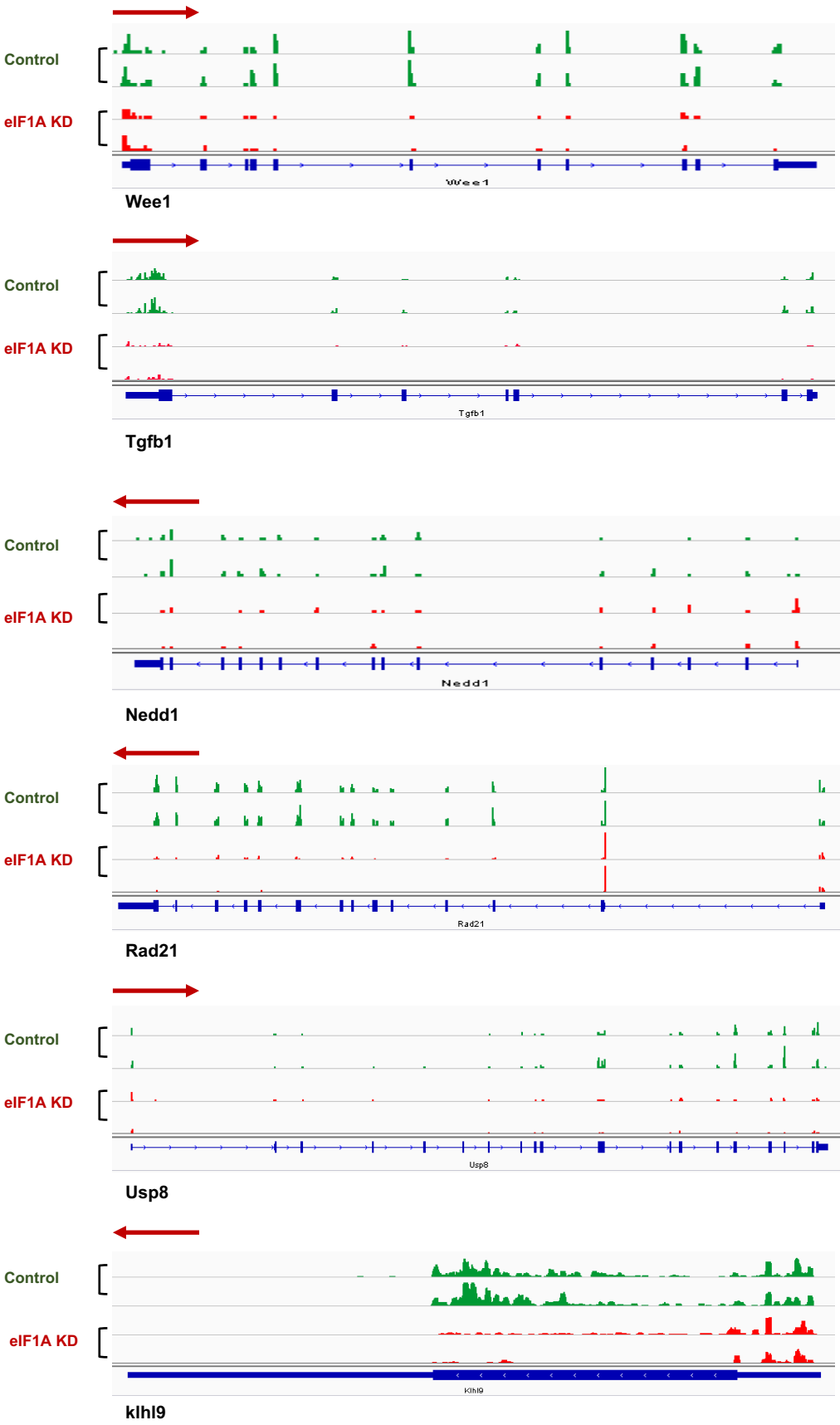


Figure 4

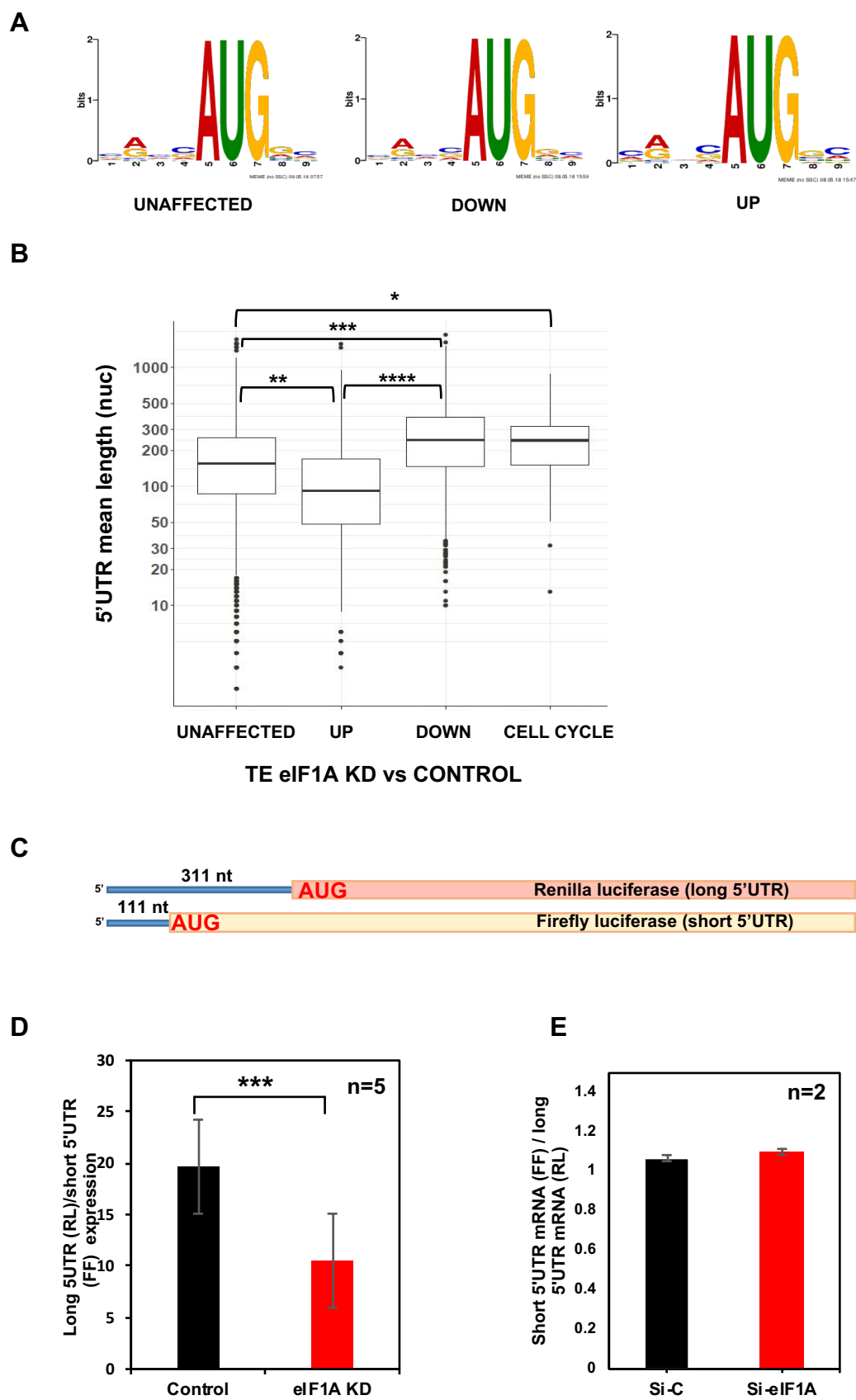


Figure 5

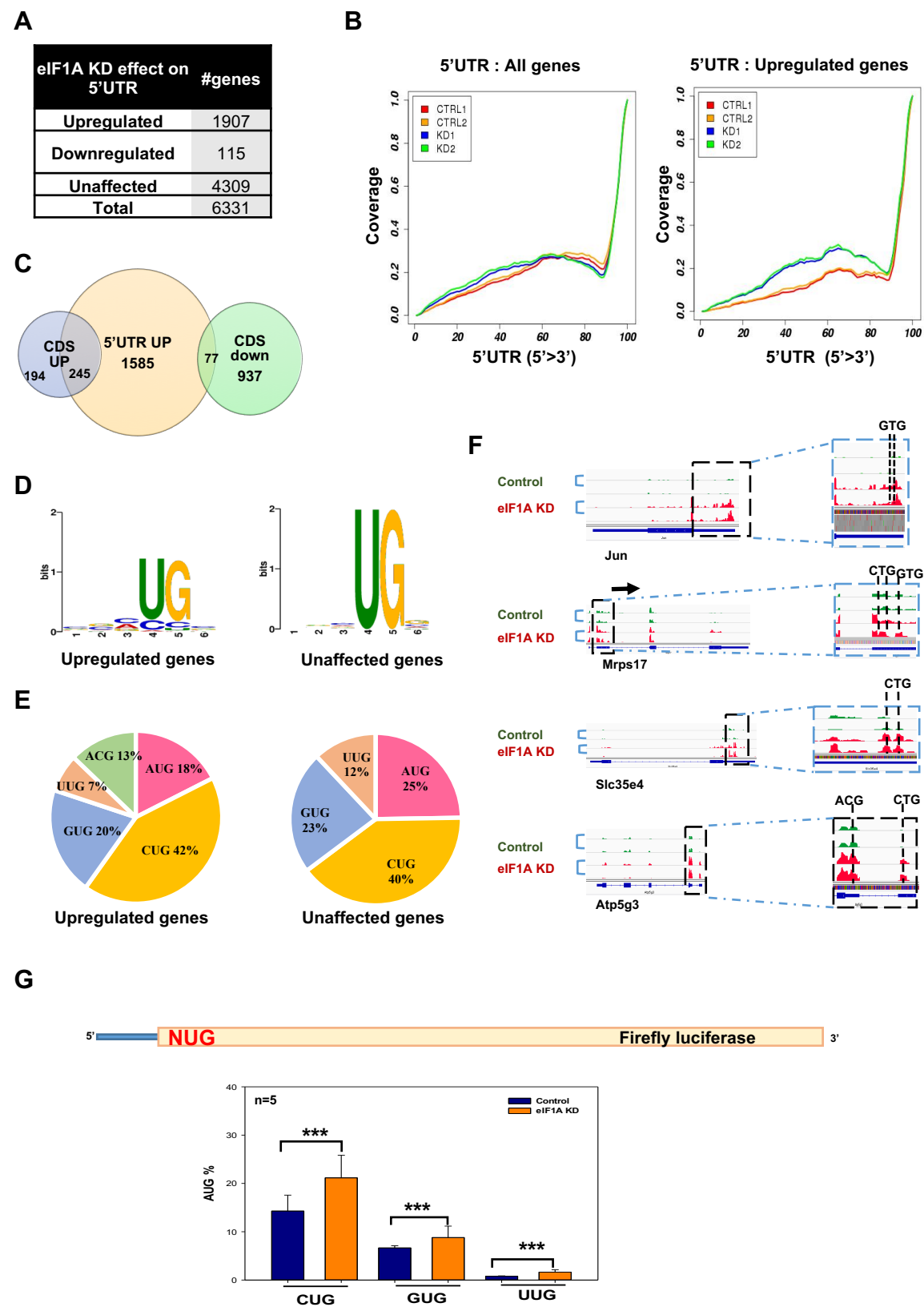
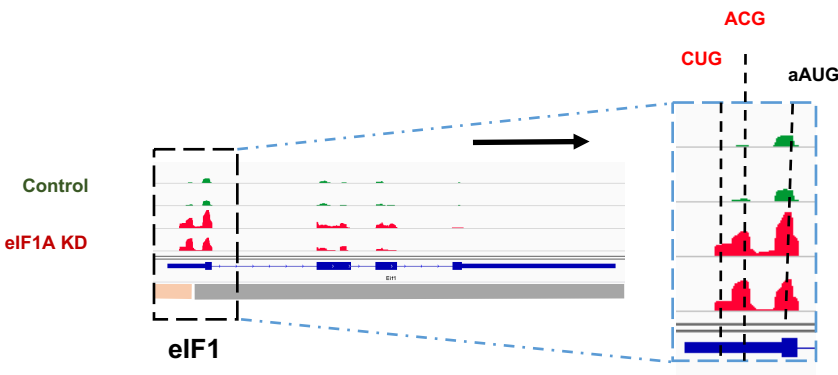
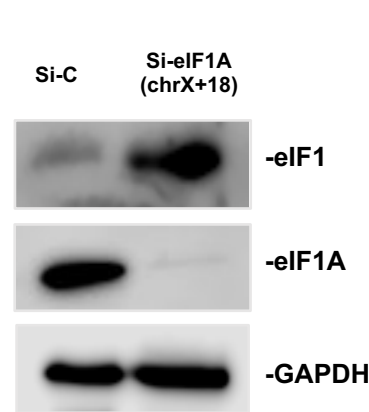


Figure 6

A



B



C

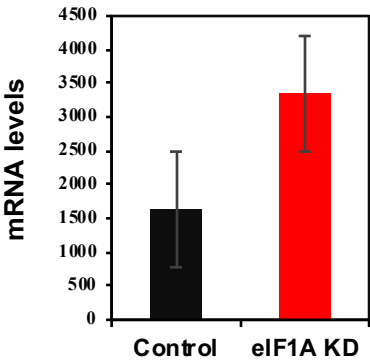


Figure 7

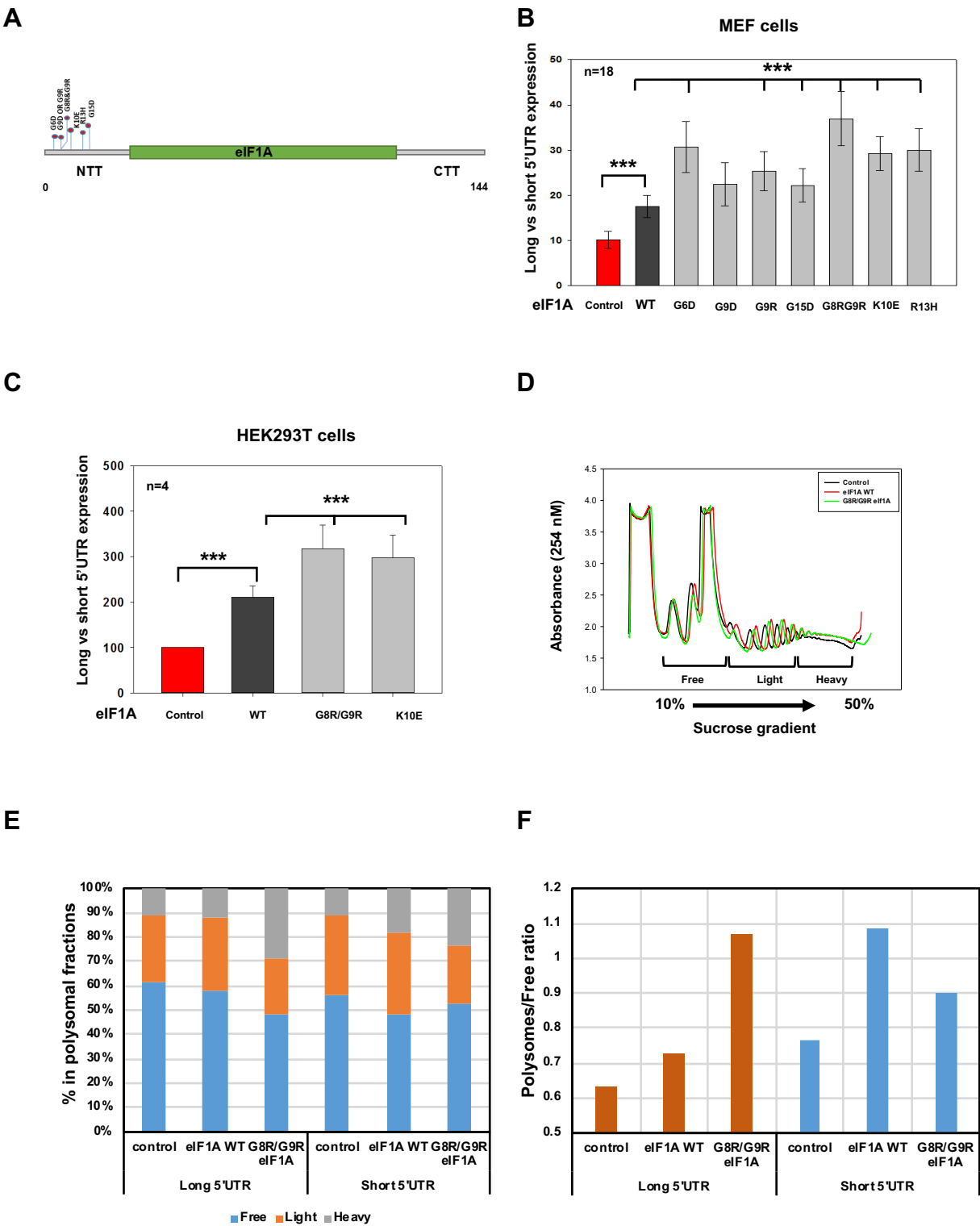
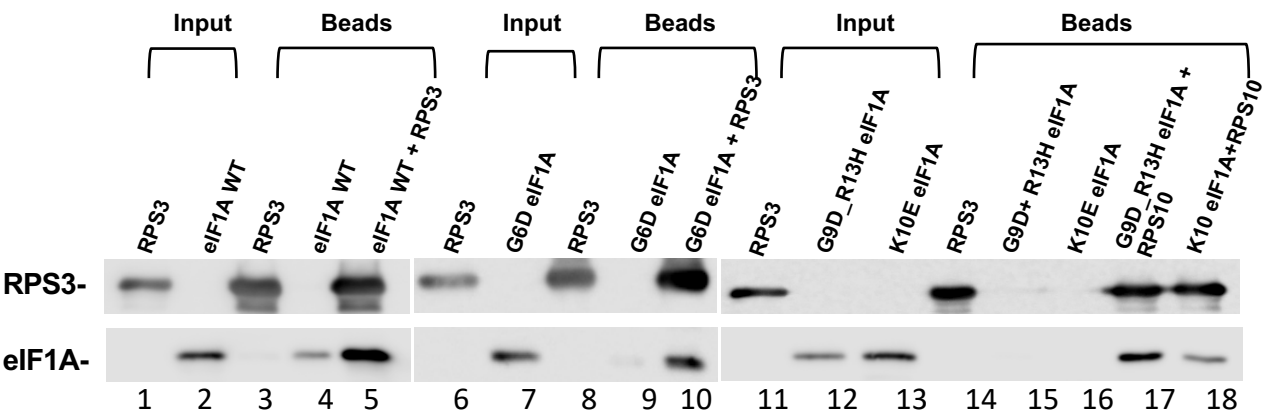
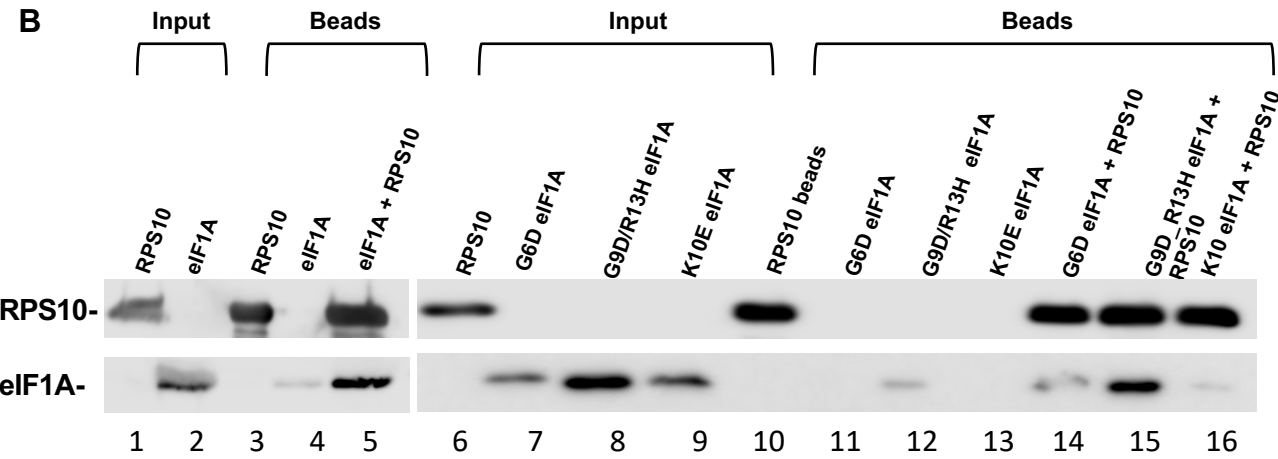


Figure 8

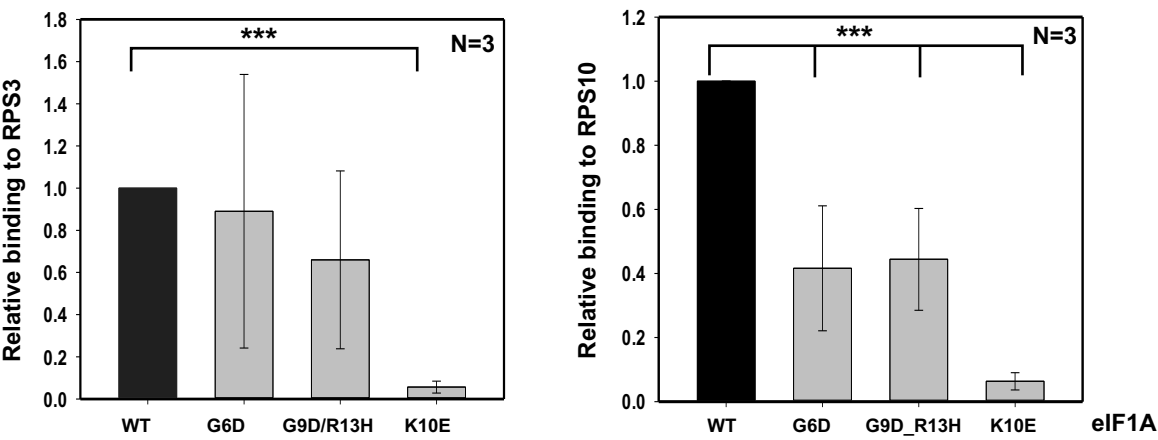
A



B



C



Supplementary figure legends

Figure S1: eIF1A depletion dramatically affects the global translation. Cell lysates of MEFs treated with siControl (black) or si-eIF1A (red) cells were subjected to sucrose gradient sedimentation and fraction collection to obtain polysome profiles.

Figure S2: Validation of eIF1A knockdown in the ribosome profile. Tracks showing the ribosome profiling reads along eIF1A (18) and eIF1AX mRNAs for replicate samples of each Control (green) and eIF1A KD (red).

Figure S3: Control and eIF1A KD cells were analyzed by western blot with antibodies against eIF1A, GAPDH and the indicated eIFs and ribosomal proteins.

Figure S4: Box plot showing relation between the 5'UTR length and translation efficiency in eIF1A KD vs control samples for 5'UTR UP genes, CDS UP genes and genes that have both 5'UTR and CDS UP.

Figure S5: eIF1A NTT mutants have minor effect on translation through non-cognate AUG. Bar graph showing expression of CUG with respect to AUG upon expression of various eIF1A mutants in MEFs as described in Fig. 5G.

Figure S1

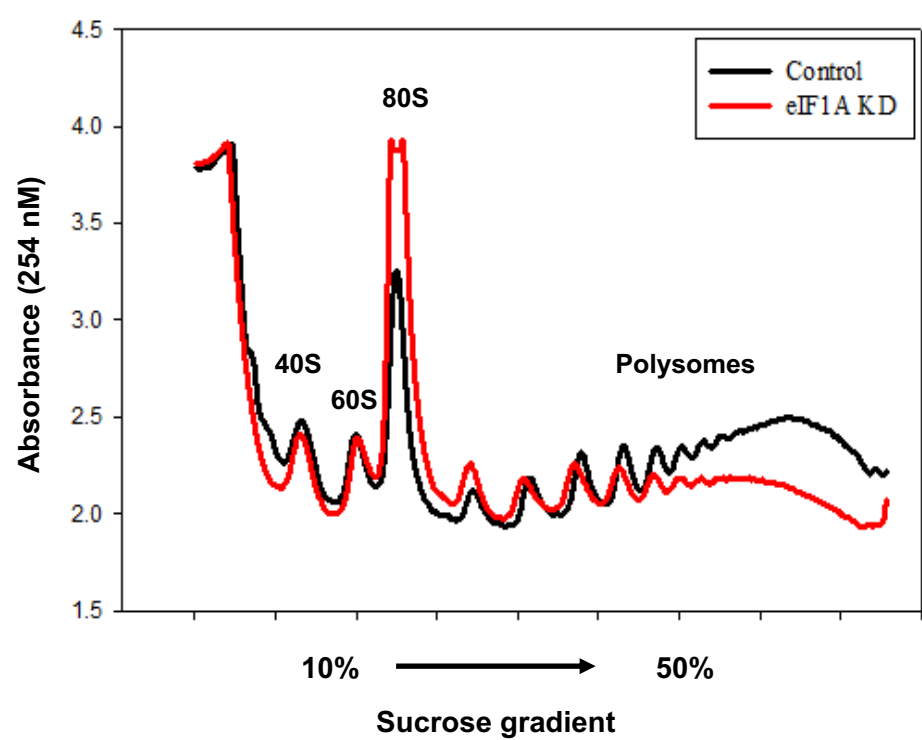


Figure S2

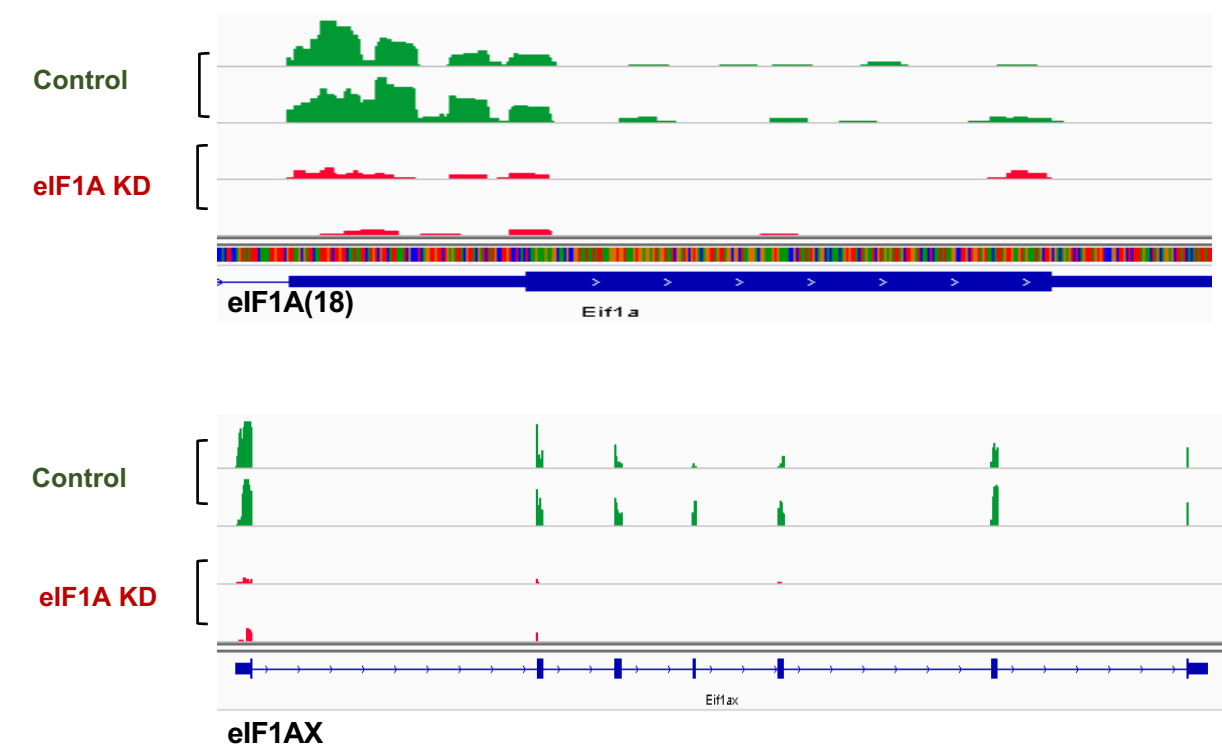


Figure S3

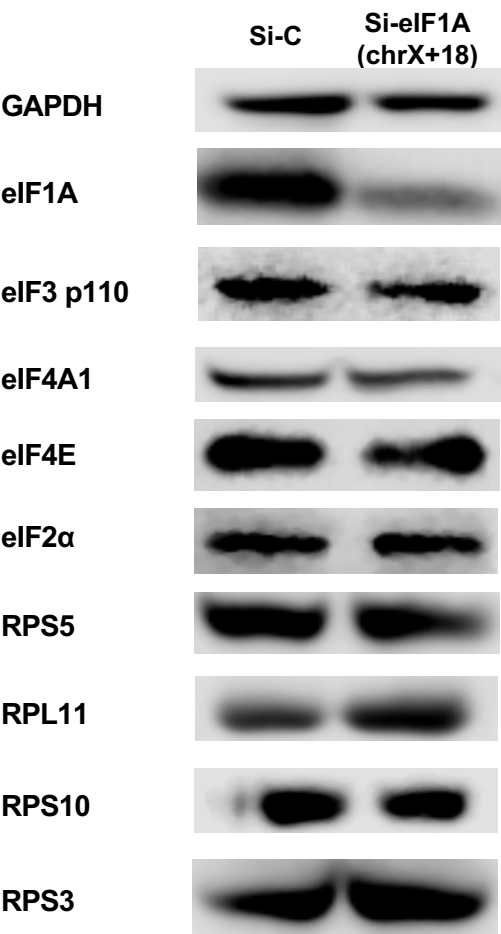


Figure S4

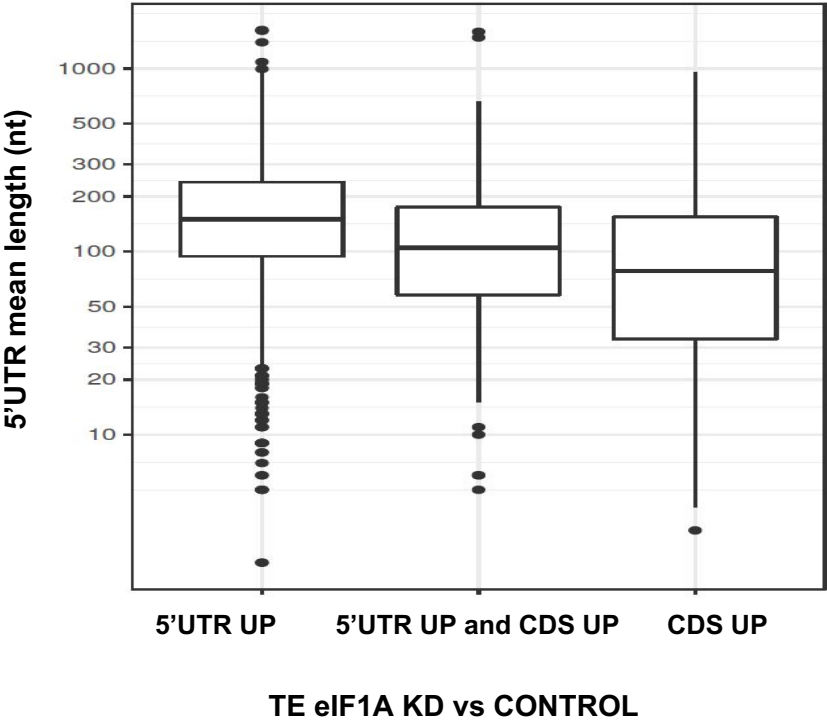


Figure S5

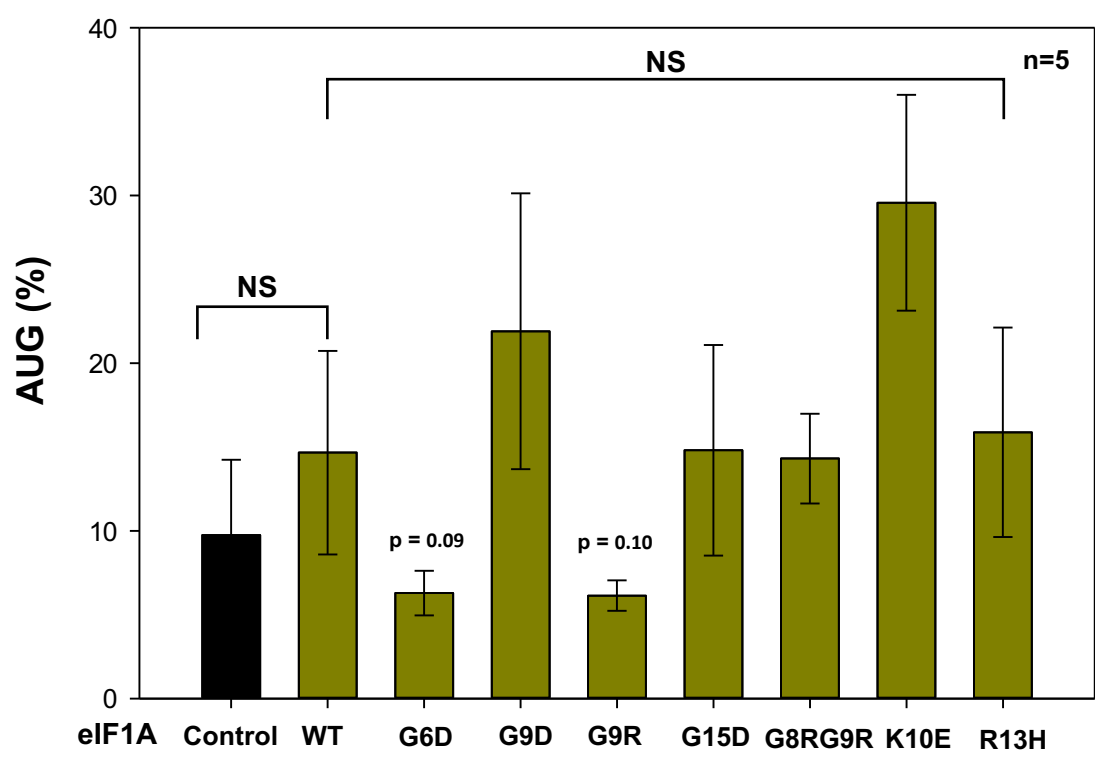


Table S1: The effect of eIF1A knockdown on the mTOR-sensitive TOP mRNAs

mTOR affected genes	Effect of eIF1A KD on gene expression
Rps10	UP
Rps11	UP
Rps12	UP
Rps13	UP
Rps14	UP
Rps15	UP
Rps21	UP
Rps23	UP
Rps24	UNCHANGED
Rps25	UP
Rps26	UP
Rps27a	UNCHANGED
Rps27l	UNCHANGED
Rps28	UP
Rps29	UP
Rps3	UNCHANGED
Rps3a1	UNCHANGED
Rps5	UP
Rps6	UNCHANGED
Rps6ka1	UNCHANGED
Rps6ka3	DOWN
Rps6ka5	UNCHANGED
Rps6kc1	UNCHANGED
Rps7	UP
Rps8	UP
Rps9	UNCHANGED
Rpsa	UP
Rpl10	UP
Rpl10a	UP
Rpl11	UNCHANGED
Rpl12	UNCHANGED
Rpl13	UP
Rpl13a	UNCHANGED
Rpl14	UP
Rpl15	UP
Rpl17	UNCHANGED
Rpl18	UP
Rpl18a	UP
Rpl35a	UP
Rpl36	UP
Rpl36a	UNCHANGED
Rpl36al	UP
Rpl7l1	UNCHANGED
Rpl8	UP
Rpl9	UNCHANGED
Rplp0	UP
Rplp1	UP
Rplp2	UP
Eif1	UNCHANGED
Eif1ad	UNCHANGED
Eif1b	UNCHANGED
Eif2b1	UNCHANGED
Eif2b3	UNCHANGED
Eif2b4	UNCHANGED
Eif2b5	UNCHANGED
Eif2d	UNCHANGED
Eif2s2	UNCHANGED
Eif2s3x	UNCHANGED
Eif3a	UNCHANGED
Eif3b	UNCHANGED
Eif3m	UNCHANGED
Eif4a1	UNCHANGED
Eif4a3	UNCHANGED
Eif4b	UNCHANGED
Eif4e	UNCHANGED
Eif4e2	UNCHANGED
Eif4enif1	UNCHANGED
Eif4h	UNCHANGED
Eif5	UNCHANGED
Eif5a	UNCHANGED
Eif6	UNCHANGED

Table S2: The effect of eIF1A knockdown on translational upregulated mRNAs upon eIF2-alpha serine 51 phosphorylation.

eIF2α activated genes	Effect of eIF1A KD on gene expression
ATF4	UNCHANGED
ATF5	UNCHANGED
ATF6	UNCHANGED
Impact	UNCHANGED
CHOP	UNCHANGED
GCN2	Down
GADD34	UP

Table S3: primers list

Primer Name	Application	sequence
GAPDH Forward	real-time PCR	AGGTCGGTGTGAACGGATTTG
GAPDH Reverse	real-time PCR	GGGGTCGTTGATGGCAACA
eIF1A (Chr18) Forward	real-time PCR	GTTGCCCTTTCCATCATGCC
eIF1A (Chr18) Reverse	real-time PCR	ACACCGTCAAAGCACATTGC
eIF1AX forward	real-time PCR	GTGACCAGCCTCTCCTGAGC
eIF1AX Reverse	real-time PCR	GGAAGTGCAGTGACTCCGA
eIF1A G6D forward	Site directed mutagenesis	CAAGAATAAAGATAAAGGAGGTAAAAAC
eIF1A G6D Reverse	Site directed mutagenesis	GGCATTTAGATGTCATCAATATC
eIF1A G9D forward	Site directed mutagenesis	GGTAAAGGAGATAAAAAACAGAC
eIF1A G9D Reverse	Site directed mutagenesis	TTTATTCTTGGGCATTTAG
eIF1A G9R forward	Site directed mutagenesis	AGGTAAAGGACGTAAAAACAGACG
eIF1A G9R Reverse	Site directed mutagenesis	TTATTCTTGGGCATTTAGATG
eIF1A G8R_G9R forward	Site directed mutagenesis	TAAAGGTAAACGACGTAAAAACAGACGCAG
eIF1A G8R_G9R Reverse	Site directed mutagenesis	TTCTTGGGCATTTAGATG
eIF1A G15D forward	Site directed mutagenesis	CAGACGCAGGGATAAGAATGAGA
eIF1A G15D Reverse	Site directed mutagenesis	TTTTTACCTCCTTTACCTTTATTCTTG
eIF1A K10E forward	Site directed mutagenesis	TAAAGGAGGTGAAAACAGACGCAG
eIF1A K10E Reverse	Site directed mutagenesis	CCTTTATTCTTGGGCATTTAG
eIF1A R13H forward	Site directed mutagenesis	TAAAAACAGACACAGGGGTAAAGAATG
eIF1A R13H Reverse	Site directed mutagenesis	CCTCCTTTACCTTTATTCTTG
eIF1A Forward	PCR cloning	CATCACCATCATCACCACAGCCAGGATCCGATGC CCAAGAATAAAGGTA
eIF1A Reverse	PCR cloning	TCGACTTAAGCATTATGCGGCCGCAAGCTTTTAG ATGTCATCAATATCTTCATC
RPS3 Forward	PCR cloning	ATGGCAGTGCAAATATCCAAG
RPS3 Forward	PCR cloning	TCGACTTAAGCATTATGCGGCCGCAAGCTTTTAT GCTGTGGGGACTGGCTGGGGCA
RPS10 Forward	PCR cloning	CATCACCATCATCACCACAGCCAGGATCCGATGT TGATGCCTAAGAAGAAC
RPS10 Forward	PCR cloning	TCGACTTAAGCATTATGCGGCCGCAAGCTTTTACT GAGGTGGCTGACCACGTCC